Gold nanocages entering into the realm of high-contrast photoacoustic ocular imaging

Raveendran, Sreejith; Lim, Hoong-Ta; Maekawa, Toru; Vadakke Matham, Murukeshan; Sakthi Kumar, D.

2018

Raveendran, S., Lim, H.-T., Maekawa, T., Vadakke Matham, M., & Sakthi Kumar, D. (2018). Gold nanocages entering into the realm of high-contrast photoacoustic ocular imaging. Nanoscale, 10(29), 13959-13968. doi:10.1039/c8nr02866d

https://hdl.handle.net/10356/137061

https://doi.org/10.1039/C8NR02866D

Gold Nanocages Entering into the Realm of High-contrast Photoacoustic Ocular Imaging

Sreejith Raveendran[a], Hoong-Ta Lim[b], Toru Maekawa[a], Murukeshan Vadakke Matham[b], D. Sakthi Kumar[a*]

[a]*Bio-Nano Electronics Research Centre, Graduate School of Interdisciplinary New Science, Toyo University, 2100, Kujirai, Kawagoe, Saitama 350-8585, Japan.*

[b]*Centre for Optical and Laser Engineering, School of Mechanical and Aerospace Engineering, Nanyang Technological University, 50 Nanyang Avenue, Singapore 639798.*

[*]Email: sakthi@toyo.jp / mmurukeshan@ntu.edu.sg

CORRESPONDING AUTHORS:

Prof. D. Sakthi Kumar,
Bio-Nano Electronics Research Centre, Graduate School of Interdisciplinary New Science,
Toyo University, 2100, Kujirai, Kawagoe, Saitama 350-8585, Japan
Email: sakthi@toyo.jp
Tel: +81 49 239 1375 (Off); Fax: +81 49 234 2502

Prof. Murukeshan Vadakke Matham,
Centre for Optical and Laser Engineering, School of Mechanical and Aerospace Engineering, Nanyang Technological University, 50 Nanyang Avenue, Singapore 639798.
Email: mmurukeshan@ntu.edu.sg
Tel: (+65) 6790 4200

ABSTRACT

Bioinert gold nanoparticles of various shapes and functionalities are widely accepted as contrast agents (CAs) for several modalities of imaging, viz., electron microscopy, computerized tomography (CT), X-ray and photoacoustic (PA) imaging. However, testing of novel compact-imaging probes for ocular diagnostic imaging is always challenging. Here, ultra-fast microwave oven synthesized gold nanocages (AuNcgs) were successfully demonstrated for high-contrast PA ocular imaging for the first time. Methods are described for the synthesis, characterization and application of quickly- synthesized AuNcgs in diagnostic ocular imaging. PA and ultrasound (US) images were acquired using a commercial US imaging scanner integrated with a tunable nanosecond pulsed laser. This integrated hybrid-modality system is a combined PA and US platform for imaging that enabled acquiring of complementary structural and optical absorption-based information simultaneously. Initial experiments were conducted using tubings filled with solutions of different concentrations of quickly- synthesized AuNcgs. Biological PA and US imaging were demonstrated using enucleated porcine eye samples. Based on the acquired results it is envisaged that AuNcgs can be employed as a high strength PA CA to potentially diagnose ocular disease like uveal melanoma in the near future.

Key Words: gold nanocages; photoacoustic imaging; ocular imaging; nanoparticles; high-contrast agents; bioimaging

1. Introduction

Ocular imaging is highly critical for the diagnosis, therapy and analysis of the severity and progression of eye diseases[1]. Several modalities in optical imaging are supplementing the most established ophthalmic imaging techniques like ultrasonography[2,3], angiography[2], and fundus photography.[1] Moreover, development of ophthalmic photoacoustic imaging (PAI) has demonstrated a safe and high-resolution visualization of deep tissue structures of eye including the retina, choroid and optic nerve.[2] PAI is a fast-growing biomedical imaging technique that has been configured to overcome the penetration depth limit of optical imaging modalities, which was of the order of ~1 mm in human tissues or skin[4]. Recently, PAI has been reported to perform deep tissue imaging of up to several centimeters[5,6].

PAI has been employed in biomedical imaging for various applications as it provides rich contrast based on the absorption heterogeienties[7]. The complementary structural and functional information provided by PAI can help clinicians to make accurate disease diagnosis. Blood is a common photoacoustic (PA) endogenous absorbers[8], which can be imaged to reveal tissue vasculature[9] and determine total hemoglobin concentration and saturation of blood oxygen.[8,10] Several exogenous contrast agents (CAs) like nanoparticles,[11–13] organic dyes[14] and fluorescent proteins[15] are also used to provide enhanced contrast of specific targets during PAI. Gold (Au) is commonly used as the coating material for biomedical PAI as it is biocompatible.[12,16] The peak absorption of such metal nanoparticles can be tuned over a broad spectrum from the near-ultraviolet to the mid-infrared,[12,17] by several ways such as altering its shape[14] (aspect ratio) and the relative dimensions of the core and shell.[17,18]

PA phenomenon is a hybrid combination of optical excitation and acoustic detection. It occurs when the sample absorbs some of the energy from the pulsed ultraviolet (UV), visible light or near-infrared excitation.[19] The energy absorbed by the sample causes an increase in transient temperature, followed by thermoelastic expansion. This produces an initial pressure rise forming broadband acoustic waves (PA waves),[8,18,20] which can be detected by an ultrasound transducer (UST). The initial pressure rise P_0 can be described using:

$$P_0(\lambda) = \Gamma F(\lambda)\mu_\alpha(\lambda), \quad (1)$$

where P_0 is directly proportional to the unitless Grüneisen parameter Γ, fluence F of the excitation wavelength λ, and optical absorption coefficient μ_α.[18,21]

Here, we are using gold nanocages (AuNcgs) synthesized via ultra-fast microwave assisted method[22] as PA CA in ocular imaging for the first time, demonstrated using enucleated porcine eye

models. Conventionally produced AuNcgs have been established as a high-contrast PA agent for imaging tumors and cancers *in vivo*.[23–27] However, its applications and possibilities in ocular imaging is far overlooked. The time-consuming conventional synthesis of AuNcgs has limited its wide application in optical imaging and theranostic studies. We have developed an ultra-fast synthesis method for AuNcgs using microwave oven heating technology, which drastically reduced the synthesis time from several hours to few seconds.[22,28] Washed AuNcgs were primarily subjected to several morphological and chemical characterizations prior to acquiring PA images.

In this paper, we have employed the quickly-synthesized AuNcgs developed by our novel method, which are first tested to show that they can generate PA waves under pulsed optical excitation. In order to demonstrate the effect of concentration on PA signal strength, different concentrations of AuNcg solutions were added into separate tubings. Also, the AuNcgs are used as PA CA in ocular imaging for the first time and demonstrated using enucleated porcine eye models. The synthesized AuNcgs are injected into the eye models to simulate and show its potential use as high strength PA CAs for disease diagnosis of diseases, such as uveal melanoma. Uveal melanoma is a type of intraocular cancer that is generally found in the iris, choroid, and ciliary body. An early diagnosis of this condition can help the patient from developing painful eye condition leading to vision loss and in certain cases of deaths due to metastasis. [29,30] It was reported that bioconjugated AuNcgs were demonstrated for its use as CAs in cancer cell imaging. [30]

2. Results and Discussion

Synthesis and Characterization of Quickly-synthesized AuNcgs

On reacting AgNcbs with 5 ml of 0.1 mM $HAuCl_4$ solution, pale-violet colored AuNcg solution was obtained. Highly monodispersed hollow AuNcgs were harvested after microwave assisted synthesis and several washing steps. Figure 1 illustrates the morphological and structural characterization of AuNcgs using high-resolution transmission electron microscopy (HRTEM). Figure 1a shows the HRTEM image of an individual AuNcg with holes in the faces and corners with corresponding fast Fourier transform (FFT) image being shown in the inset. Transmission electron microscopy (TEM) characterization revealed the hollow nature of the AuNcg showing a thick-walled cubical box pattern. The wall thickness of AuNcgs was measured to be 5±2 nm with an average edge length of ≈65 nm. Atomic resolution image of one of the corners of AuNcg was recorded and presented in Figure 1b. Line profile of the FFT data generated shows the interplane distance of the Au crystal (Fig. 1c). Line profile (Fig. 1d) of the well-defined lattice fringes from the selected area of Figure 1B shows a d-spacing of 2Å, which can be indexed to {200} planes of the Au fcc structure.[31] Depending upon the degree of passivation by PVP over AuNcgs, the dispersity of the nanocages

differ (Fig. 1e). However, on thorough washing and ultrasonication, relatively monodispersed AuNcgs were collected. Furthermore, high-angle annular dark-field scanning transmission electron microscopy (HAADF-STEM) images (Figs. 1f-g) allow the evolution of AuNcgs with holes from solid AgNcbs in a uniform fashion to be monitored. Transmission electron microscopy-energy dispersive spectroscopy (TEM-EDS) mappings of AuNcgs reveal the homogenous alloy distribution of Au and Ag (Figs. 1h-k). However, the semi-quantitative assessment of atomic percentage of Au and Ag shows a successful galvanic displacement of Ag from the initial AgNcb template. Figure 1m shows the EDS spectrum of constitutive elements present in the AuNcg analyzed.

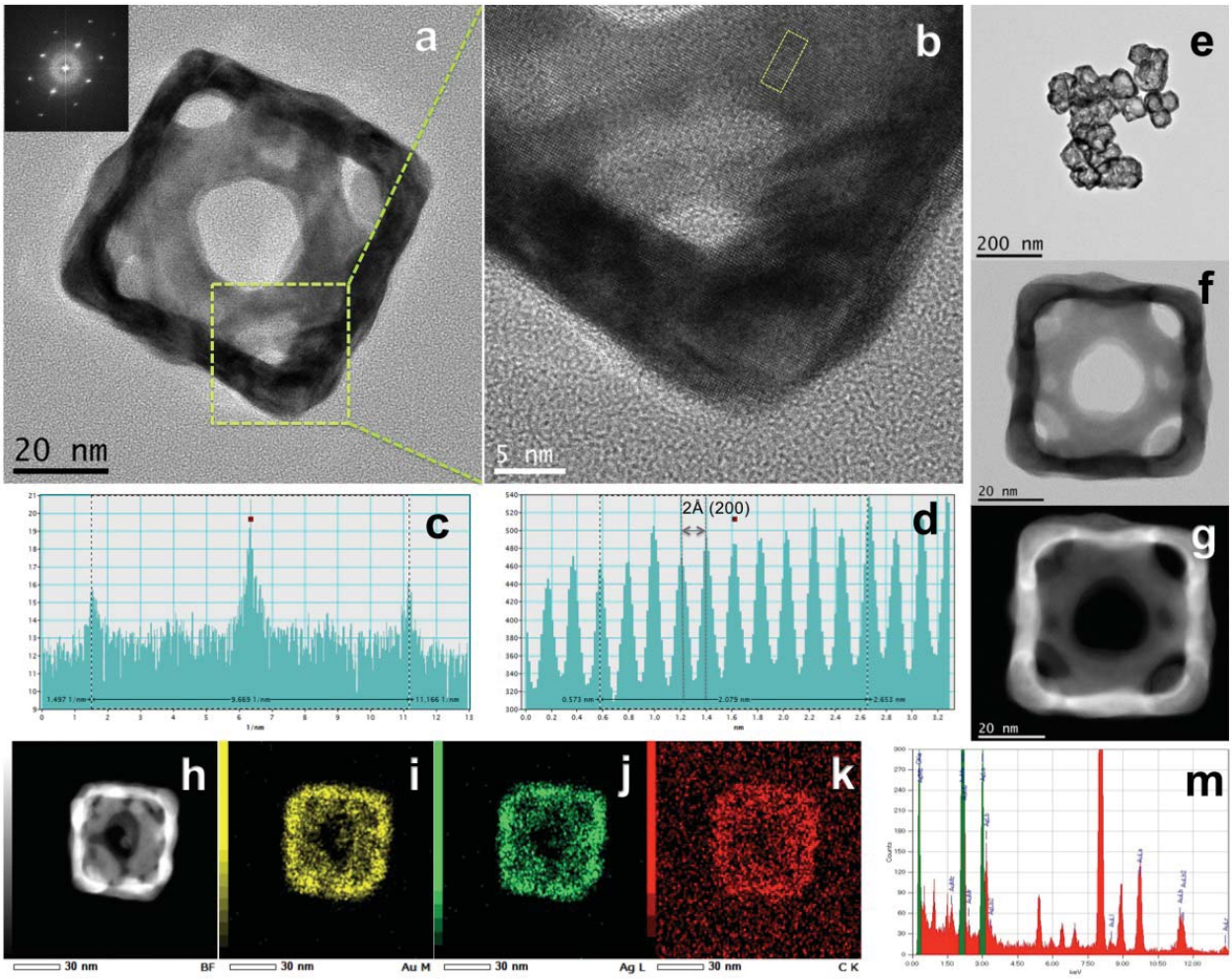

Figure 1: HRTEM characterization of quickly- synthesized AuNcgs. a, HRTEM image of AuNcg; Corresponding FFT image for the AuNcg (Inset); **b,** HRTEM image of the corner of AuNcg shown in figure **a**; **c,** Line profile of FFT image shown in figure **a**-inset; **d,** Line profile from the highlighted area of the HRTEM image of AuNcg shown in figure **b**; **e,** low magnification TEM image of AuNcgs in cluster; **f,** High magnification bright field TEM image of AuNcg **; g,** HAADF-STEM image of AuNcg shown in **f**; **h- k,** EDS mapping images for AuNcg: **h-** Bright field; **i-** Au; **j-** Ag; **k-** C; **m,** EDS spectrum showing the constitutive elements in AuNcgs.

Further morphological characterization was performed using Scanning electron microscopy (SEM), Ultraviolet-visible (UV-Vis) spectroscopy and X-ray powder diffraction (XRD). SEM image shows well-dispersed, corner truncated AuNcgs with pores in the faces and corners (Fig. 2a). Inverted gray scale SEM image show transparent white zones that correspond to the holes present in AuNcgs (Fig. 2b). UV-Vis spectra of AuNcgs show the tunability of localized surface plasmon resonance spectra

in the near-infrared region, which highly favors the optical properties of the AuNcgs produced (Fig. 2c). The evolution of hollow AuNcgs from solid AgNcbs shifts the localized surface plasmon resonance peak towards the near-infrared region, which offers several optical properties to AuNcgs[32]. XRD spectrum of quick-synthesized AuNcgs (Fig. 2d) was compared with JCPDS data for pure Au standard (00-004-0784) and AgCl standard (00-031-1238).

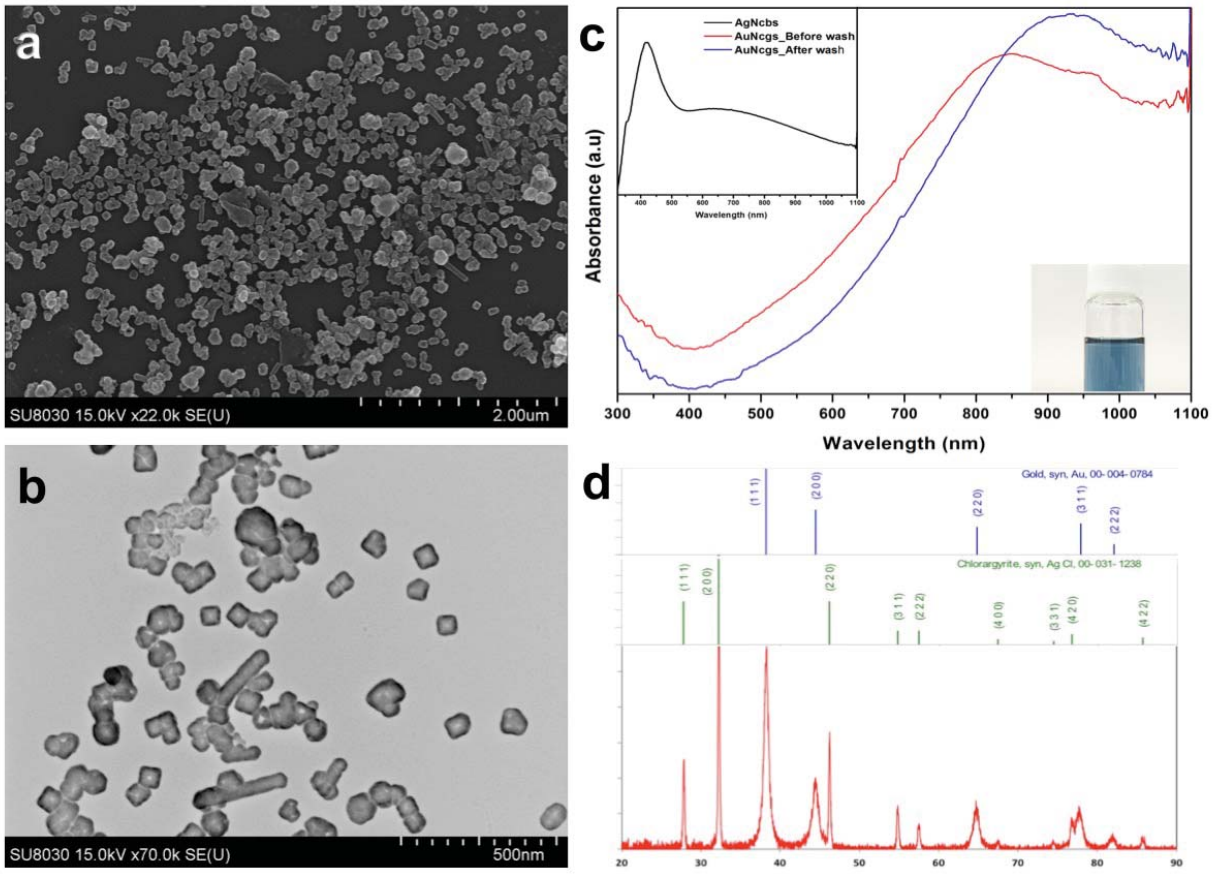

Figure 2: : SEM, UV-vis, and XRD characterization of quickly- synthesized AuNcgs. a, SEM image of AuNcgs; **b,** inverted- alpha SEM image of AuNcgs; SEM images demonstrates that the AuNcgs synthesized via microwave aided ultrafast method yields nanocages of uniform size and shape, however, certain clumps of nanoparticles were observed that was dispersed upon thorough washing. **c**, UV-vis absorption spectra for AgNcbs and AuNcgs synthesized: AuNcgs-before wash (red), AuNcgs- after wash (blue), AgNcbs (inset), Photograph of AuNcg solution after washing (inset); Upon washing the excess, unbound polymer and impurities of AgCl was washed off, which enhanced the spectral intensity of AuNcgs with a red shift of the peak centre. **d**, XRD spectra of AuNcgs synthesized using microwave oven method showing the peaks (111), (200), (220), (311) and (222). The spectrum (red) represents the peaks arising from AuNcgs and the AgCl impurities present in the mixture of nanocage sample. Based on the spectra, the intensity of (111) is relatively high compared to the (200) peak, showing that the AuNcg has a slight corner truncation, which is evident from the TEM and SEM images as well. Corresponding standard XRD spectra for Au (Blue) and AgCl (Green) were depicted above for comparison. Standard spectra was taken from JCPDS database.

Verification of generation of PA signals

The experimental setup to capture PA signals generated by various concentrations of quick-synthesized AuNcgs is shown in Figure 3a. AuNcg sample solution was serially diluted as mentioned in the method section and placed in a cuvette before PA signals were acquired. Data processing was performed and some of the processed signals can be seen in Figure 3b.

The mean and standard deviation of the processed UST signal (indicating the strength of PA), at varying concentrations of the AuNcg solution are plotted against the concentration, as shown in

Figure 3c. The line of best fit with zero-intercept is also plotted. The slope of the line of best fit and R^2 value were determined to be 1.0235 and 0.9938, respectively. The R^2 value of 0.9938 (which is close to 1) indicates that the experimental data are very close to the line of best fit. The gradient of the line of best fit of 1.0235 indicates that the amplitude of the PA waves detected by the UST is directly proportional to the concentration of the AuNcg solution. This is consistent with Eqn. (4) (see **Methods**) and proves that the signals acquired from the experiment were due to the PA waves generated by the AuNcg solution.

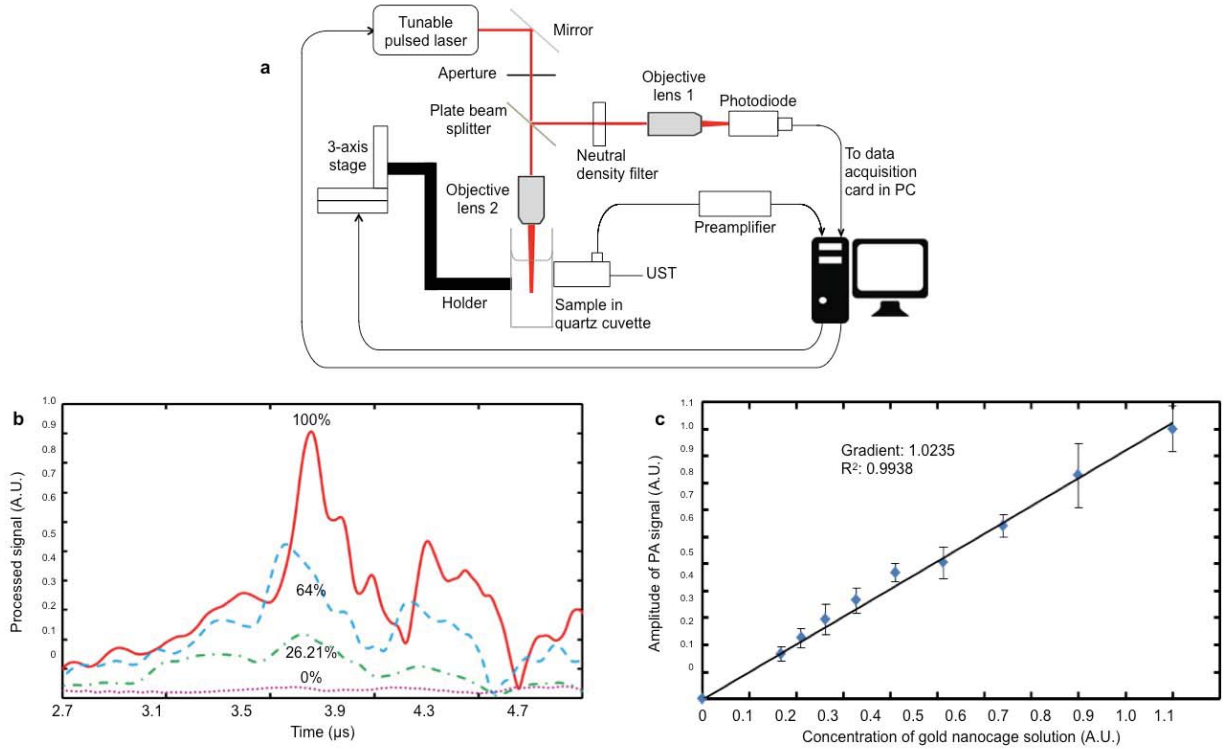

Figure 3: PA experiments with AuNcg solution in quartz cuvette. a, Experimental setup. **b,** PA signals after Hilbert transformation. PA signals of larger amplitude were observed when the concentration of the AuNcg solutions were higher. **c,** Experimental results for verification of generation of PA signals by AuNcg solution in quartz cuvette. The line of best fit between the PA amplitude and the concentration of AuNcg solution has a gradient of about 1. This is in line with Eqn. (4) in **Methods** and verifies that the quickly-synthesized AuNcgs can produce PA waves and potentially be used as a PA CA.

PAI of varying concentrations of AuNcg solution in tubings

The experimental setup shown in Figure 4a used to acquire PA and ultrasound (US) images of the test samples. In order to illustrate the effect of AuNcg concentration, PA/US images of the separate tubings, each filled with AuNcg solutions of different concentrations, are shown in Figure 4d. In the Figures 4b-c, the left tubing was filled with deionized water, the center tubing was filled with a mixture of deionized water and AuNcg solution (1:1 volumetric ratio) and the right tubing was filled with AuNcg solution alone. The tubings were excited individually for acquiring PA signals. The combined PA/US images can be seen in the Figure 4d.

It can be seen from Figure 4d (i) that a weak PA signal was acquired from the top of the left tubing. In Figure 4d (ii), a weak PA signal was also acquired from the top of the center tubing, but two other PA signals were also observed from the top and bottom of the internal section of the tubing.

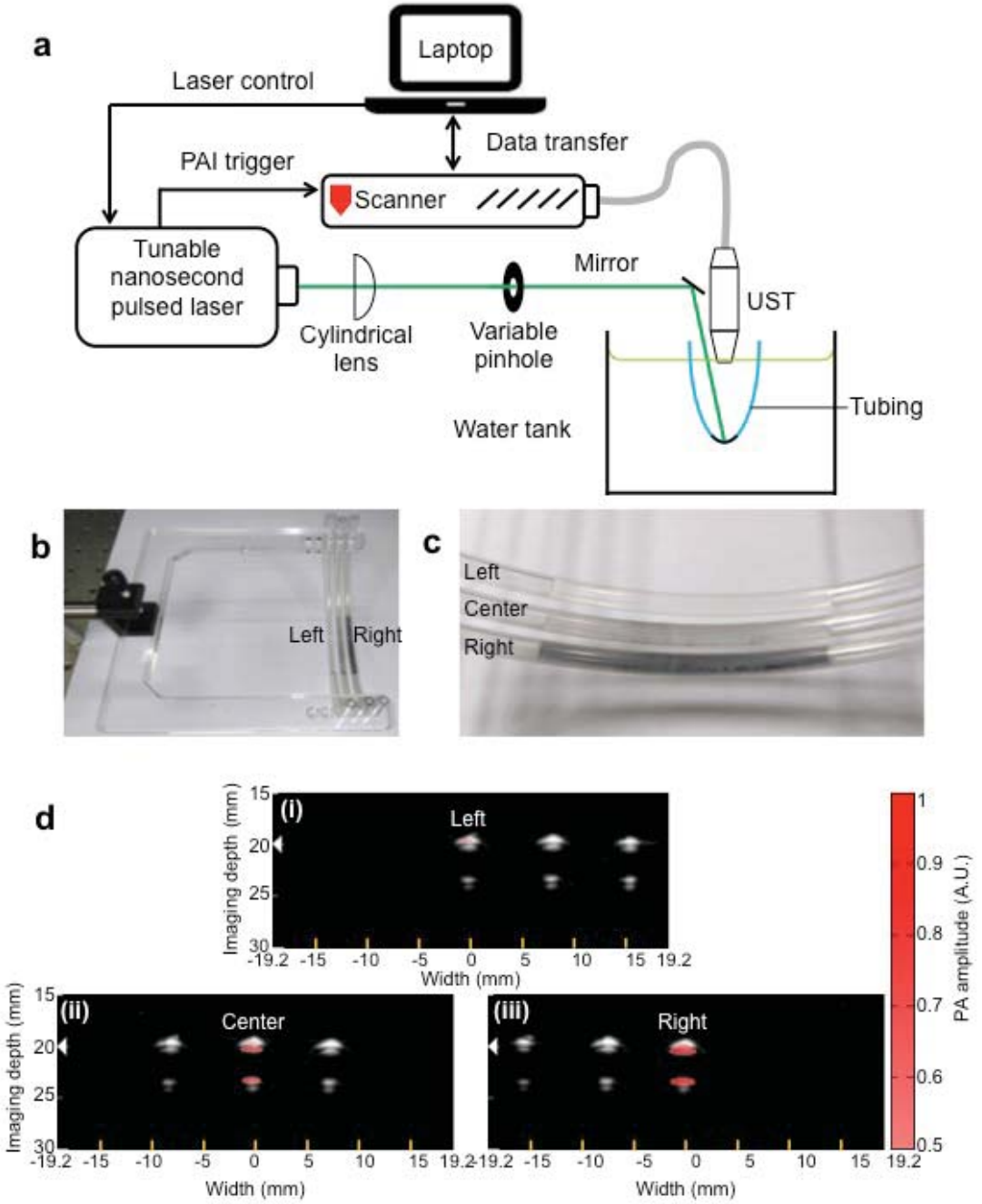

Figure 4: PAI of varying concentrations of AuNcg solutions in tubings. a, PAI experimental setup. **b,** Acrylic holder to hold the three tubings in place. **c,** Close-up of the three tubings. The left tubing was filled with deionized water. It has no AuNcg and the tubing appears to be clear. The center tubing was filled with a mixture of deionized water and AuNcg solution, thus it appears darker compared to the left tubing due to the presence of AuNcgs in the mixture. The right tubing was filled with AuNcg solution. It had the highest concentration of AuNcg solution and appears to be the darkest among the three tubings. **d,** Combined PA/US images when each tubing was separately illuminated for PAI. **(i),** The left tubing was filled with deionized water and when excited, a weak PA signal can be observed from the tubing. **(ii),** The center tubing was filled with a mixture of deionized water and AuNcg solution. When excited, two strong PA signals are observed from the internal section of the tubing, which are attributed to the presence of AuNcgs in the solution. **(iii),** The right tubing was filled with AuNcg solution and when excited, the PA signals are similar to those shown in (ii), but of larger amplitude and more intense. This is attributed to the solution in the right tubing with a higher concentration of AuNcg. These show that the AuNcgs enhance PA signals and the PA enhancement increases with the concentration of the AuNcg solution.

The same was observed in Figure 4d (iii), but PA signals from the internal section of the right tubing are observed to be larger in amplitude and more intense. The PA signals from the internal section of the center and right tubings are attributed to the presence of AuNcgs in the solution in the tubings.

Two areas are selected from the center tubing where PA signals are observed (top and bottom of tubing's internal section). From the interrogation area of ~0.35×0.35 mm^2, the values are selected and averaged to represent the strength of the PA signals due to the AuNcgs. The same was done for the right tubing. The representative strength of the PA signals from the center tubing to that of the right tubing has a ratio of 0.827:1, which is not proportional to the AuNcg concentration in the tubings of 0.5:1. This could be due to how the PA images are presented by the system, where the algorithms used may not be linear (approximate log compression). However, the trend of a higher AuNcg concentration giving stronger PA signals still holds.

PAI of enucleated porcine eye samples with AuNcg as CA

Figures 5a and 5b shows the image of enucleated porcine eye used for PA imaging and illustrative image of eye, respectively. Two sets of imaging were carried out for each eye sample. The first set of imaging produced a set of PA and US images representing a healthy eye sample (i.e. before the introduction of AuNcgs into the eye), as shown in Figures 5c, BEFORE (i- iv). The second set of imaging was done after the injection (Figs. 5c AFTER (i- iv) of AuNcg solution into the eye, just above the iris.

By comparing the schematic diagram of the eye (Fig. 5b) to the combined PA/US images of the eye samples (Figs. 5c), it can be observed that the structural features of the eye are revealed by the US image. The different parts of the eye such as cornea, anterior chamber, lens, iris and posterior pole can be seen. The combined images before and after the injection of AuNcg solution for each eye sample are shown side-by-side (Figs. 5c). It can be observed that PA signals were generated from the iris on the left.

An area of ~0.35×0.35 mm^2 was selected as the interrogation region and each set of 50 PA images was considered for the analysis. These areas were selected from the excited iris region where PA signals were produced. The amplitudes of the PA signals within each area were average to represent the strength of the PA signals as presented by the system. PA signals were detected from the pigmented iris before the introduction of AuNcgs, due to the presence of melanin, which is optically absorbing.[33] It was found that after the injection of AuNcg solution into the region above the left iris of the eye samples, the PA signals for eye samples 1 to 4 increased by 46.3 ±14.3 %, 81.4 ±16.7 %, 57.9 ±14.8 % and 17.6 ±17.2 %, respectively (Fig. 5d). These results show that the AuNcgs can

potentially be used as a PA CA in ocular imaging. Specific targeting of AuNcgs to markers of diseases can potentially be used to identify diseases[30] such as uveal melanoma by using PAI as the imaging (diagnostic) modality.

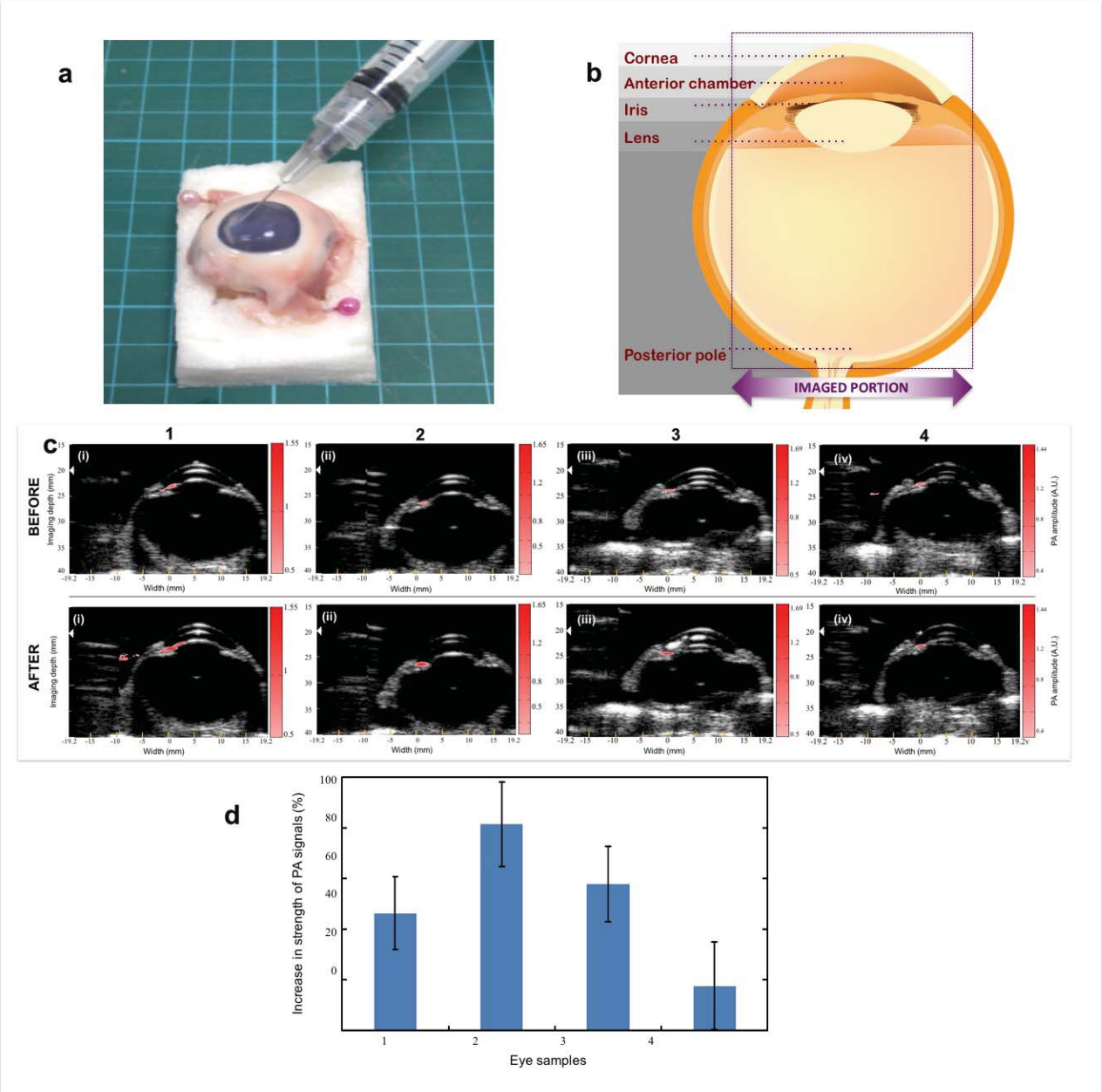

Figure 5: PAI of enucleated porcine eye samples with AuNcg. a, Injection of AuNcg solution into porcine eye sample. **b,** Schematic diagram of eye. **c,** Combined images of eye samples 1, 2, 3 and 4. Images, 'BEFORE' **(i)- (iv)** shows the eye samples 1- 4 before injection of AuNcg solution respectively. . Images, 'AFTER' **(i)- (iv)** shows the eye samples 1- 4 after injection of AuNcg solution respectively**,** Eye samples before injection showed very little background PA signals due to melanin pigments , however the PA signals measured after the injection of AuNcg solution was drastically increased in intensity. The injected AuNcgs were used to simulate the binding of bio-conjugated AuNcgs on uveal melanoma in the iris region. It can be observed that after the introduction of AuNcg, the strength of the PA signals in the iris increases and becomes more intense. This demonstrates that the quickly-synthesized AuNcgs can potentially be used to create contrast enhancement in PA images for ocular disease diagnosis. **d,** Increase in strength of PA signals after injection of AuNcg solution. After the introduction of AuNcg solution into the eye, the amplitude of the PA signals in eye samples 1, 2, 3 and 4 increased by 46.3%, 81.4%, 57.9% and 17.6%, respectively. The average increase in the amplitude of the PA signal is about 50.8%.

3. Conclusions

Highly efficient AuNcgs were synthesized using microwave oven heating technology as an ultra-fast method in the production of AuNcgs.[22] Quickly-synthesized AuNcgs were characterized using HRTEM, SEM, XRD and UV-Vis spectroscopy and were found uniform in size and shape. It was observed that the UV-Vis absorption spectra of quickly-synthesized AuNcgs was spanning across

the near-infrared region, which is highly beneficial for several optoelectronics and high contrast imaging applications. Here, we have demonstrated a detailed instrumentation for the PA experiments performed using the quickly- synthesized AuNcgs produced via microwave heating technology for the first time. Preliminary studies were conducted to determine the ability of quickly-synthesized AuNcgs to generate PA signals similar to conventionally synthesized and reported AuNcgs.[24] This study was conducted using different concentrations of the quickly-synthesized AuNcg solutions. The results show that the strength of the PA signals is directly proportional to the concentration of the AuNcg solution and verified that PA signals were generated by the AuNcgs under pulsed optical excitation. In the subsequent study, high contrast PA images were captured with varying concentrations of AuNcgs in separate tubings. A commercial US imaging scanner, integrated with a tunable nanosecond pulsed laser was used as the imaging platform; it has a UST set within a clinical-style imaging probe for convenient handling. The acquired PA images showed that tubings with higher concentrations of AuNcg solutions will result in the detection of stronger PA signals. The source of the PA signals can also be compared by referring to its corresponding US images, which provide structural information of the imaged region. AuNcgs were used as PA CA for the first time in ocular imaging. PA and US images were acquired from the enucleated porcine eye models and was followed by the injection of the quickly-synthesized AuNcgs into the eye models to simulate uveal melanoma condition. Another set of PA and US images were acquired and compared to the set of images acquired prior to the injection of AuNcgs. The results show that the approximately 50.8 % increase in the strength of the PA signals (increased by 17.6 % to 81.4 %) was observed after AuNcgs were introduced into the eye models. This demonstrates that the quickly-synthesized AuNcgs can potentially be used to create contrast enhancement in PA images for ocular disease diagnosis. Uveal melanoma is a type of intraocular cancer that is generally found in the iris, choroid, and ciliary body. An early diagnosis of this condition can help the patient from developing painful eye condition leading to vision loss and in certain cases of deaths due to metastasis[29,30]. It was reported that bioconjugated AuNcgs were demonstrated for its use as CAs in the cancer cell imaging.[30] It is envisaged that, based on the analysis presented in this manuscript, quickly- synthesized AuNcgs can be used as a high strength PA CA to potentially diagnose uveal melanoma. A future improvement to the hybrid-modality imaging system is to integrate the laser excitation with clinical-style imaging probe. This removes the need to adjust the position of the laser excitation when the imaging probe is moved to image another region. Integrating the PA and US images of the eye models makes hybrid-modality imaging possible, to form combined PA/US images to provide complementary structural and optical absorption-based information. This allows the source of the PA signals to be known by referring to the structural information provided by the US images. Using the AuNcgs as markers of uveal

melanoma in hybrid-modality imaging can help to determine the size (spread and depth) and location of uveal melanoma relative to other ocular structures. This can help clinicians make better diagnostic evaluation and confirmation of diseases.

4. Experimental Section

Chemicals and instruments

Polyvinylpyrollidone ($M_w \approx 55{,}000$) (Cat.#856568), sodium sulfide nonahydrate (Cat.#208043) and gold (III) chloride trihydrate (Cat.#G4022-1G) were procured from Sigma-Aldrich, Japan. Ethylene glycol (Cat.#14114-00) and silver nitrate (Cat.#37075-30) were purchased from Kanto chemicals, Japan. All other chemicals and reagents used were of analytical grade.

AuNcgs were characterized using Scanning Electron Microscope (SEM), High Resolution Microscope-Transmission Electron Microscope (HRTEM), X-ray powder diffraction (XRD) and Energy-Dispersive X-Ray Spectroscope (EDS). SEM images were taken using Hitachi, SU6600. TEM images were recorded with JEOL, HRTEM (JEM-ARM200F, 200 kV) fitted with EDS (JEOL, DrySD100GV). UV-Vis absorption spectra of as-synthesized AgNcbs and AuNcgs were measured with Beckman Coulter Spectrophotometer (DU730). XRD spectra were recorded using RIGAKU X-ray diffractometer (SmartLab9kW) and data was compared with Joint Committee on Powder Diffraction Standards (JCPDS) database.

PAI experiments were conducted using following instruments: Nanosecond pulsed laser (Vibrant 355 II, Opotek Inc.), Power mater (Nova Display and 12A-V1, Ophir), Beamsplitter (BSW10, Thorlabs), Neutral density filter (ND30A, Thorlabs), Objective lens 1 (UPlan FLN 10x, Olympus), Objective lens 2 (MPlan N 5x, Olympus), Photodiode (SM05PD2B, Thorlabs), digitizer (200 MS/s, Razor CompuScope 1622, GaGe), 3-axis stage (T-LS28M, Zaber Technologies), UST (V110-RM, Olympus Panametrics-NDT), Pre-amplifier (5662, Olympus Panametrics-NDT) and US imaging scanner (UltraVision 64B Research Platform, Winprobe) with clinical-style imaging probe (L8, Winprobe).

Microwave mediated synthesis of AuNcgs

AgNcbs were synthesized based on the microwave assisted polyol method mentioned elsewhere.[28] Briefly, 10 ml of ethylene glycol (EG) solution of 250 μM Na_2S was vigorously stirred after adding 0.075 M PVP. The mixture was injected drop wise using a syringe into a 10 ml of EG solution of $AgNO_3$ (0.05 M) under constant magnetic stirring. On addition, the solution turned wine colored due to the formation of Ag_2S. Wine colored solution was intermittently heated (stop and start

method) in a microwave and swirled manually for thorough mixing between the heating steps. Heating experiment was conducted in a microwave oven (YJ-50H8, LG Electric, Japan) operating at frequency of 50 Hz, power consumption of 1000 W and rated high frequency output of 500 W. Khaki-colored solution containing AgNcbs were formed within seconds of reaction. Nanocubes were washed several times before galvanic replacement with $HAuCl_4$ solution. Galvanic replacement reaction was conducted using 5 ml of 0.1 mM $HAuCl_4$ solution with 550 µl of as-synthesized AgNcbs in microwave oven.[22] AgNcb solution was first mixed with 5 ml of 9 mM aqueous solution of PVP before introducing Au solution. The mixture was heated in the microwave oven intermittently until a stable pale-purple color was obtained. AuNcgs were washed several times with water and ethanol/water 1:1 mixture by volume and dispersed in deionized water for characterization and PAI studies.

Concentration of the AuNcg solutions was measured using Inductively Coupled Plasma Mass Spectrometry (ICP-MS), based on the quantification of Au (III) ions present in various test AuNcg solutions. ICP-MS measurement was performed using iCAP-Q, Thermo Scientific with a plasma Ar flow rate of 15 L/min and a dwell time of 100 ms for each sample. All the samples were microwave (ETHOS UP) digested using 5% aqua regia. A series of Au standard solution were prepared and measured for obtaining a calibration curve, using which the Au (III) concentrations in the test samples were found.

Experimental setup for the verification of generation of PA signals by AuNcg solution in cuvette

The AuNcg reported in this paper was suspended in deionized water. In order to prove that the AuNcg solution was able to produce PA signals, an experiment measuring AuNcg solutions of varying concentrations was conducted. The optical absorption coefficient of a solution is dependent on its concentration *Conc* and molar absorption ε_α, as seen in Eqn. (2). Substituting Eqn. (2) into Eqn. (1) gives Eqn. (3). Considering that only an excitation wavelength λ is used, the Grüneisen parameter Γ and ε_α are constants and the measurements are corrected for fluence F fluctuations, Eqn. (3) is reduced to Eqn. (4). Equation (4) shows that if the AuNcg is able to produce PA signals, the strength of the PA signals is directly proportional to its concentration.

$$\mu_\alpha(\lambda) = Conc \cdot \varepsilon_\alpha(\lambda), \quad (2)$$

$$P_0(\lambda) = \Gamma F(\lambda) Conc \cdot \varepsilon_\alpha(\lambda), \quad (3)$$

$$P_0 \propto Conc, \quad (4)$$

The experimental setup to capture the PA signals for this purpose consisted of a tunable nanosecond pulsed laser at 800 nm with a frequency of 10 Hz (Vibrant 355 II, Opotek Inc.) to provide the required optical excitation for PA measurement. The pulse energy was measured to be ~26 μJ using a power meter (Nova Display and 12A-V1, Ophir). When the pulse reached the beamsplitter (BSW10, Thorlabs), the reflected light was directed towards the neutral density filter (ND30A, Thorlabs) and focused by objective lens 1 (UPlan FLN 10x, Olympus) onto the photodiode (SM05PD2B, Thorlabs). The pulse detected by the photodiode triggered the digitizer (200 MS/s, Razor CompuScope 1622, GaGe). The transmitted light through the beamsplitter travelled towards objective lens 2 (MPlan N 5x, Olympus) before reaching the AuNcg solution placed in a quartz cuvette (104-10-40, Hellma Analytics), which was held in place by a 3-axis stage (T-LS28M, Zaber Technologies). Upon excitation, the PA wave was detected by the UST (V110-RM, Olympus Panametrics-NDT), which was in direct contact with the quartz cuvette. A pre-amplifier (5662, Olympus Panametrics-NDT) with a 54 dB gain amplified the detected signal before being directed to the digitizer. When the digitizer was triggered, the signals from both the photodiode measuring the fluence of the pulsed excitation and UST measuring the strength of the PA waves were acquired. The signals were averaged over 100 pulses for each measurement to improve the signal-to-noise ratio. A custom developed LabView® software was used to control the laser, 3-axis stage, digitizer, and to save the averaged data. 5 measurements were acquired for each concentration of AuNcg solution.

The quartz cuvette was initially filled with 1.5 ml of the AuNcg solution using a single-channel pipettor (4075, Lambda^{TM} Plus Corning). The initial concentration of the AuNcg solution was 100% and with this concentration, measurements were carried out for 5 times. This is continued for a total of 9 concentrations: 100%, 80%, 64%, 51.2%, 40.96%, 32.77%, 26.21%, 20.97% and 16.78%. A control experiment was also carried out with 0% AuNcg concentration using only deionized water. A total of 50 measurements (5 for each of 10 concentrations) were acquired.

Experimental setup for PAI of varying concentrations of AuNcg solution in tubings

PA and US images of the tubings filled with solutions of different AuNcg concentrations were acquired using a commercial US imaging scanner (UltraVision 64B Research Platform, Winprobe) which was integrated with a tunable nanosecond pulsed laser (Vibrant 355II, Opotek Inc). The experimental setup is shown in Figure 4a. This reported integrated system[3] enabled hybrid-modality imaging where PA and US images can both be acquired to provide combined images of complementary structural and optical absorption-based information. The images were acquired using a 128-element linear array UST set within a clinical-style imaging probe (5-10 MHz, L8, Winprobe). The elements had a pitch of 0.3 mm, thus the UST had an azimuthal length of 38.4 mm

for US imaging. For PAI, the azimuthal length was only 19.2 mm as only the center 64 elements in the UST were used. The UST produced US pulses and the detected echoes formed US images. The imaging scanner formed multiple US images and waited for the PA trigger from the laser. The PA trigger cause the scanner to stop producing US pulses and the detected UST signals were used to form a PA image. Thereafter, the UST produced US pulses and USI resumed. This process was repeated and PA and US images were produced at 10 Hz and ~40 Hz, respectively.

Three transparent flexible plastic tubings (S3 E-3603, Tygon) were used in this experiment. They have inner and outer diameters of 3.2 mm and 4.8 mm, respectively. They were held in place from the ends and placed at ~7.5 mm apart using an acrylic holder (Fig. 4b). The left tubing was filled with deionized water, the center tubing was filled with a mixture of deionized water and AuNcg solution (1:1 volumetric ratio) and the right tubing was filled with AuNcg solution only (Fig. 4c). They were then left to settle for ~30 minutes.

During the experiment, the tubings were partially submerged in the water and the linear-array UST was placed transverse to and above the lowermost point of the three tubings. PA excitation was delivered to one tubing at a time. This helped to ensure that constant excitation fluence was delivered to each tubing. In order to get PA signals in this experiment, the excitation beam with wavelength of 500 nm and diameter of 5 mm was used. The pulse energy was measured to be ~590 μJ using a power meter (Nova Display and 12A-V1, Ophir). First, the left tubing which was placed below the UST was excited and PA images were taken. This is followed by exciting the center and right tubings to obtain the relevant PA images. 50 PA and 50 US images were captured when each tubing was imaged.

Experimental setup for PAI of enucleated porcine eye samples with AuNcg as CA

Biological PA and US images of enucleated porcine eye samples were also acquired using the same system as mentioned in the above section. The eye samples were held in place by a holder and aligned to face upwards. The eyes were positioned towards the right of the UST so that the left iris appeared at the center of the images. The UST was placed ~2 cm above the lens of the eye.

Two sets of imaging were conducted by taking 50 PA and 50 US images of the porcine eye samples. In this study, the laser beam with wavelength of 500 nm and diameter of 3 mm was used for excitation at the iris. The pulse energy was measured to be ~71 μJ using a power meter (Nova Display and 12A-V1, Ophir). The first imaging produced a set of PA and US images, which represents that of a healthy eye sample. It was then removed from the water tank and ~0.15 ml of AuNcg solution was slowly injected into the eye, just above the iris on the left (Fig. 6A). The eye was then left untouched for ~20 minutes so that the AuNcg solution can settle. These simulated

samples, prepared following the above procedure represent uveal melanoma, which is tagged by bio-conjugated AuNcgs.

Preparation of porcine eye samples

Four porcine eye samples (*Sus scrofa domestica*) were used in this study. The porcine eye samples with extraocular tissues removed were acquired from local abattoir. The samples were placed on ice until the experiments began. Samples that were found to be free from any signs of deterioration after visual inspection were used for experiment. The eye samples were used within 6 hours of death. The study was conducted according to NTU's regulations on biosafety and the regulations of Agri-Food & Veterinary Authority of Singapore.

PA and US data processing

Verifying generation of PA signals by AuNcg solution in cuvette: Data acquired from the experiments were processed offline using in-house written script in MATLAB®. Data processing started with Hilbert transformation of the UST signals and correction for fluence fluctuations using signals from the photodiode (Fig. 3b). Hilbert transformation is widely used in analytical signal analysis to pick up the envelopes of vibration signals.[34] These signals were corrected for any background PA signals using the mean value of the signal from the sample with 0% AuNcg concentration. The mean and standard deviation of the measurements of the concentrations were calculated and normalized.

PAI of AuNcg solution in tubings and porcine eye samples: Data acquired from the experiments were processed offline using in-house written script in MATLAB®. Each set of 50 PA and 50 US images were averaged to form a representative image with reduced random noises. Signals of weak intensity in the representative PA images were also removed for better clarity. For each eye sample, the two representative PA images were normalized with respect to the strongest signal in the PA image before the AuNcg solution was introduced.

Acknowledgments

S. Raveendran, T. Maekawa and D.S. Kumar would like to acknowledge their sincere gratitude to the Ministry of Education, Culture, Sports, Science and Technology (MEXT), Japan for the financial support under the program of the strategic research foundation at private universities S1101017, organized by the MEXT, Japan. H.T. Lim and V.M. Murukeshan acknowledge the financial support received through COLE-EDB funding and RG 162/15 (Ministry of Education, Singapore).

406 **Conflict of Interest**

407 The authors declare no conflict of interest

408 # References

409 1 J. S. Wolffsohn and L. N. Davies, *Expert Rev. Ophthalmol.*, 2007, **2**, 755–767.

410 2 A. de la Zerda, Y. M. Paulus, R. Teed, S. Bodapati, Y. Dollberg, B. T. Khuri-Yakub, M. S.
411 Blumenkranz, D. M. Moshfeghi and S. S. Gambhir, *Opt. Lett.*, 2010, **35**, 270–272.

412 3 H.-T. Lim and M. V. Matham, *J. Med. Imaging*, 2015, **2**, 36003.

413 4 L. V Wang, *Nat. Photonics*, 2009, **3**, 503–509.

414 5 S. Mallidi, G. P. Luke and S. Emelianov, *Trends Biotechnol.*, 2011, **29**, 213–221.

415 6 L. V. Wang and S. Hu, *Science (80-.).*, 2012, **335**, 1458–1462.

416 7 Y. Jin, C. Jia, S.-W. Huang, M. O'Donnell and X. Gao, *Nat. Commun.*, 2010, **1**, 41.

417 8 M. R. Chatni, J. Xia, R. Sohn, K. Maslov, Z. Guo, Y. Zhang, K. Wang, Y. Xia, M. Anastasio, J.
418 Arbeit and L. V Wang, *J. Biomed. Opt.*, 2012, **17**, 76012.

419 9 Y. Wang, X. Xie, X. Wang, G. Ku, K. L. Gill, D. P. O. Neal, G. Stoica and L. V Wang, *Nano Lett.*,
420 2004, **4**, 1689–1692.

421 10 M. L. Li, J. T. Oh, X. Y. Xie, G. Ku, W. Wang, C. Li, G. Lungu, G. Stoica and L. V Wang, *Proc.*
422 *Ieee*, 2008, **96**, 481–489.

423 11 B. Wang, A. Karpiouk, D. Yeager, J. Amirian, S. Litovsky, R. Smalling and S. Emelianov, *Opt. Lett.*,
424 2012, **37**, 1244.

425 12 C. Loo, A. Lin, L. Hirsch, M.-H. Lee, J. Barton, N. Halas, J. West and R. Drezek, *Technol. Cancer*
426 *Res. Treat.*, 2004, **3**, 33–40.

427 13 K. A. Homan, M. Souza, R. Truby, G. P. Luke, C. Green, E. Vreeland and S. Emelianov, *ACS Nano*,
428 2012, **6**, 641–650.

429 14 J. Becker, A. Trügler, A. Jakab, U. Hohenester and C. Sönnichsen, *Plasmonics*, 2010, **5**, 161–167.

430 15 D. Razansky, M. Distel, C. Vinegoni, R. Ma, N. Perrimon, R. W. Köster and V. Ntziachristos, *Nat.*
431 *Photonics*, 2009, **3**, 412–417.

432 16 X. Yang, E. W. Stein, S. Ashkenazi and L. V. Wang, *Wiley Interdiscip. Rev. Nanomedicine*
433 *Nanobiotechnology*, 2009, **1**, 360–368.

434 17 M.-L. Li, J. C. Wang, J. a Schwartz, K. L. Gill-Sharp, G. Stoica and L. V Wang, *J. Biomed. Opt.*,
435 2013, **14**, 10507.

436 18 J. J. Niederhauser, M. Jaeger, R. Lemor, P. Weber and M. Frenz, *IEEE Trans. Med. Imaging*, 2005,
437 **24**, 436–440.

438 19 M. Gyawali, W. P. Arnott, R. A. Zaveri, C. Song, H. Moosm??ller, L. Liu, M. I. Mishchenko, L. W.
439 A. Chen, M. C. Green, J. G. Watson and J. C. Chow, *Atmos. Chem. Phys.*, 2012, **12**, 2587–2601.

440 20 H. F. Zhang, K. Maslov, G. Stoica and L. V. Wang, *Nat. Biotechnol.*, 2006, **24**, 848–851.

441 21 G. P. Luke, S. Y. Nam and S. Y. Emelianov, *Photoacoustics*, 2013, **1**, 36–42.

22 S. Raveendran, A. Sen, T. Maekawa and D. S. Kumar, *Nano Res.*, 2016, **10**, 1078–1091.

23 G. D. Moon, S. Choi, X. Cai, W. Li, E. C. Cho and U. Jeong, *J.Am.Chem.Soc.*, 2011, **133**, 4762–4765.

24 C. Kim, E. C. Cho, J. Chen, K. H. Song, L. Au, C. Favazza, Q. Zhang, C. M. Cobley, F. Gao, Y. Xia and L. V. Wang, *ACS Nano*, 2010, **4**, 4559–4564.

25 S. E. Skrabalak, J. Chen, L. Au, X. Lu, X. Li and Y. Xia, *Adv. Mater.*, 2007, **19**, 3177–3184.

26 S. E. Skrabalak, L. Au, X. Li and Y. Xia, *Nat. Protoc.*, 2007, **2**, 2182–2190.

27 J. Chen, J. M. Mclellan, A. Siekkinen, Y. Xiong and Z. Li, *J.Am.Chem.Soc.*, 2006, **128**, 14776–14777.

28 D. Chen, X. Qiao, X. Qiu, J. Chen and R. Jiang, *Nanotechnology*, 2010, **21**, 25607.

29 B. Damato, *Clin. Exp. Ophthalmol.*, 2004, **32**, 639–647.

30 J. Chen, F. Saeki, B. J. Wiley, H. Cang, M. J. Cobb, Z. Li, L. Au, H. Zhang and M. B. Kimmey, *Nano Lett.*, 2005, **5**, 473–477.

31 S. Liu, xusheng zheng, L. Song, W. Liu, T. Yao, Z. Sun, Y. Lin and S. Wei, *Chem. Commun.*, 2016, 6617–6620.

32 M. Hu, H. Petrova, A. R. Sekkinen, J. Chen, J. M. McLellan, Z. Y. Li, M. Marquez, X. Li, Y. Xia and G. V. Hartland, *J. Phys. Chem. B*, 2006, **110**, 19923–19928.

33 W. Liu and H. F. Zhang, *Photoacoustics*, 2016, **4**, 112–123.

34 L. Yu and V. Giurgiutiu, *Smart Struct. Syst.*, 2005, **1**, 185–215.

AUTHOR CONTRIBUTIONS

S.R., T.M., M.V.M., and D.S.K. conceived the idea and designed the project. S.R. and H.T.L. conducted the experiments and imaging studies, respectively. S.R., H.T.L., M.V.M. and D.S.K. analyzed the data. S.R., H.T.L., M.V.M. and D. S. K. wrote the paper.

FIGURE LEGENDS

Figure 1: HRTEM characterization of quickly- synthesized AuNcgs. a, HRTEM image of AuNcg; Corresponding FFT image for the AuNcg (Inset); **b,** HRTEM image of the corner of AuNcg shown in figure **a**; **c,** Line profile of FFT image shown in figure **a**-inset; **d,** Line profile from the highlighted area of the HRTEM image of AuNcg shown in figure **b**; **e,** low magnification TEM image of AuNcgs in cluster; **f,** High magnification bright field TEM image of AuNcg **; g,** HAADF-STEM image of AuNcg shown in **f**; **h- k,** EDS mapping images for AuNcg: **h-** Bright field; **i-** Au; **j-** Ag; **k-** C; **m,** EDS spectrum showing the constitutive elements in AuNcgs.

Figure 2: : SEM, UV-vis, and XRD characterization of quickly- synthesized AuNcgs. a, SEM image of AuNcgs; **b,** inverted- alpha SEM image of AuNcgs; SEM images demonstrates that the AuNcgs synthesized via microwave aided ultrafast method yields nanocages of uniform size and shape, however, certain clumps of nanoparticles were observed that was dispersed upon thorough washing. **c**, UV-vis absorption spectra for AgNcbs and AuNcgs synthesized: AuNcgs-before wash (red), AuNcgs- after wash (blue), AgNcbs (inset), Photograph of AuNcg solution after washing (inset); Upon washing the excess, unbound polymer and impurities of AgCl was washed off, which enhanced the spectral intensity of AuNcgs with a red shift of the peak centre. **d**, XRD spectra of AuNcgs synthesized using microwave oven method showing the peaks (111), (200), (220), (311) and (222). The spectrum (red) represents the peaks arising from AuNcgs and the AgCl impurities present in the mixture of nanocage sample. Based on the spectra, the intensity of (111) is relatively high compared to the (200) peak, showing that the AuNcg has a slight corner truncation, which is evident from the TEM and SEM images as well. Corresponding standard XRD spectra for Au (Blue) and AgCl (Green) were depicted above for comparison. Standard spectra was taken from JCPDS database.

Figure 3: PA experiments with AuNcg solution in quartz cuvette. a, Experimental setup. **b,** PA signals after Hilbert transformation. PA signals of larger amplitude were observed when the concentration of the AuNcg solutions were higher. **c,** Experimental results for verification of generation of PA signals by AuNcg solution in quartz cuvette. The line of best fit between the PA amplitude and the concentration of AuNcg solution has a gradient of about 1. This is in line with Eqn. (4) in **Methods** and verifies that the quickly-synthesized AuNcgs can produce PA waves and potentially be used as a PA CA.

Figure 4: PAI of varying concentrations of AuNcg solutions in tubings. a, PAI experimental setup. **b,** Acrylic holder to hold the three tubings in place. **c,** Close-up of the three tubings. The left tubing was filled with deionized water. It has no AuNcg and the tubing appears to be clear. The center tubing was filled with a mixture of deionized water and AuNcg solution, thus it appears darker compared to the left tubing due to the presence of AuNcgs in the mixture. The right tubing was filled with AuNcg solution. It had the highest concentration of AuNcg solution and appears to be the darkest among the three tubings. **d,** Combined PA/US images when each tubing was separately illuminated for PAI. **(i),** The left tubing was filled with deionized water and when excited, a weak PA signal can be observed from the tubing. **(ii),** The center tubing was filled with a mixture of deionized water and AuNcg solution. When excited, two strong PA signals are observed from the internal section of the tubing, which are attributed to the presence of AuNcgs in the

solution. **(iii),** The right tubing was filled with AuNcg solution and when excited, the PA signals are similar to those shown in (ii), but of larger amplitude and more intense. This is attributed to the solution in the right tubing with a higher concentration of AuNcg. These show that the AuNcgs enhance PA signals and the PA enhancement increases with the concentration of the AuNcg solution.

Figure 5: PAI of enucleated porcine eye samples with AuNcg. a, Injection of AuNcg solution into porcine eye sample. **b,** Schematic diagram of eye. **c,** Combined images of eye samples 1, 2, 3 and 4. Images, 'BEFORE (i)- (iv)' shows the eye samples 1- 4 before injection of AuNcg solution respectively. Images, 'AFTER (i)- (iv)' shows the eye samples 1- 4 after injection of AuNcg solution respectively, Eye samples before injection showed very little background PA signals due to melanin pigments, however the PA signals measured after the injection of AuNcg solution was drastically increased in intensity. The injected AuNcgs were used to simulate the binding of bio-conjugated AuNcgs on uveal melanoma in the iris region. It can be observed that after the introduction of AuNcg, the strength of the PA signals in the iris increases and becomes more intense. This demonstrates that the quickly-synthesized AuNcgs can potentially be used to create contrast enhancement in PA images for ocular disease diagnosis. **d,** Increase in strength of PA signals after injection of AuNcg solution. After the introduction of AuNcg solution into the eye, the amplitude of the PA signals in eye samples 1, 2, 3 and 4 increased by 46.3%, 81.4%, 57.9% and 17.6%, respectively. The average increase in the amplitude of the PA signal is about 50.8%.